Revista Mexicana de Astronomía y Astrofísica, **34**, 87–104 (1998)

A [Ne V] IMAGE, TEMPERATURE MAPS, AND NEW SPECTROSCOPIC OBSERVATIONS OF NGC 6302[1]

Joaquín Bohigas

Instituto de Astronomía
Universidad Nacional Autónoma de México

Received 1998 May 7; accepted 1998 August 19

RESUMEN

Las regiones más excitadas de la nebulosa planetaria NGC 6302 son visualizadas a la luz de [Ne V] 3426 Å. Al comparar esta imagen con la que Bohigas (1994) obtuvo para Hβ, se encuentra que el plasma de alta excitación se extiende $\sim 45''$ a ambos lados de un cinturón que divide la nebulosa, de un modo que evoca al chorro de un jet al expanderse. Inicialmente el grado de excitación decrece conforme nos alejamos del ecuador, pero posteriormente se "re-excita" en cuatro arcos bien delineados que definen una estructura bipolar. Se obtuvieron mapas de temperatura de las líneas de O^{+2} y N^{+}, y se encuentra que T[O III] es siempre mayor que T[N II], tal como se espera dado que I(He II λ4686)/I(Hβ) $\geq$ 0.25. La temperatura es menor en regiones de alta densidad. No se halló alguna correlación entre la temperatura o el cociente de temperaturas con el mecanismo de excitación (choques o fotones). Se encontró una excelente correlación entre T[N II] y T[O III]/T[N II]: el cociente es mayor a menor temperatura. Al comparar observaciones espectroscópicas de regiones con diversos grados de excitación se encuentra que los coeficientes de corrección por ionización normalmente utilizados claramente subestiman la abundancia de estados superiores de ionización. Se obtienen mejores resultados bajo el esquema sugerido para regiones donde la mayor parte del helio está doblemente ionizado, aunque esta situación no se presenta en NGC 6302.

ABSTRACT

The highly excited regions of the planetary nebula NGC 6302 are visualized with an image taken in the light of [Ne V] 3426 Å. When compared with the Hβ image taken by Bohigas (1994), the highly excited plasma is seen to extend $\sim 45''$ at both sides of a central lane bisecting the nebula, in a manner reminiscent of a jet nozzle. Excitation initially lessens away from the equatorial plane, but the gas is then "re-excited" in four well delineated arches defining a bipolar structure. Temperature maps derived from the O^{+2} and N^{+} lines were also produced, and it was found that T[O III] is always larger than T[N II], as expected since I(He II λ4686)/I(Hβ) $\geq$ 0.25. Temperatures are smaller in high density regions. There is no correlation between the temperature or the temperature ratio with the excitation mechanism (photons or shocks). A surprisingly tight correlation exists between T[N II] and T[O III]/T[N II], with the latter increasing as T[N II] decreases. Comparing spectroscopic observations of regions with different degree of excitation, it is found that "standard" ionization correction factors underestimate the abundance of higher ionization stages. Better results are obtained when using the scheme recommended for regions where most of helium is doubly ionized, though this circumstance fails to occur in NGC 6302.

Key words: **PLANETARY NEBULAE–INDIVIDUAL (NGC 6302)**

[1] Based on observations collected at the Observatorio Astronómico Nacional, San Pedro Mártir, B. C., México.

1. INTRODUCTION

Extreme physical conditions characterize the Type I (Peimbert 1978) planetary nebula NGC 6302. These are manifest in a number of lines from very highly ionized species: [Si VII] λ2.48 μm (Ashley & Hyland 1988), [Mg VIII] λ3.028 μm (Pottasch et al. 1996), and [S VIII] 9913 Å (Reconditi & Oliva 1993; this paper) are among the most prominent. These ions require very high energies (between 205 and 281 eV), and their existence has generated a controversy regarding their ionizing source. Lame & Ferland (1991) suggested that these high ionization stages are produced by shocks resulting from the fast wind of the central star, identified from the high velocity wings ($\pm$ 400 km s^{-1}) of the [Ne V] 3426 Å line (Meaburn & Walsh 1980a). This hypothesis seemed to be supported on the grounds of the large temperature ($\sim$ 70,000 K) that Rowlands, Houck, & Herter (1994) determined from the [Ne V] line ratios, some 3.5 times larger than the temperature derived from the [O III] lines and much too high to be supported with photoionization models. But new computations and higher quality data lead to a [Ne V] temperature in the vicinity of 20,000 K (Oliva, Pasquali, & Reconditi 1996; Pottasch et al. 1996), similar to the temperature determined from the [O III] lines and understandable within the framework of pure photoionization. Furthermore, Pottasch et al. (1996) reproduce most of these lines (excepting [S VIII] 9913 Å) with a spherically symmetric constant density photoionization model where the temperature of the central star is 380,000 K. The central star is heavily obscured by a toroid (Rodríguez et al. 1985), and has not yet been seen. Besides hiding the central star, the toroid determines to some extent the morphology of the nebula, which seems to be composed of more than one bipolar cavity (Meaburn & Walsh 1980b), a situation encountered in 5 more planetary nebulae (Manchado, Stanghellini, & Guerrero 1996). In a comprehensive image analysis including the most important lines from low ionization stages (up to He II λ4686), Bohigas (1994, henceforth Paper I) showed that photoionization is the main exciting mechanism at, or near, the bright central region, but that shock excitation is common throughout NGC 6302. Elongated structures diverging from the central region were identified as oblique shocks impinging on the walls of a bipolar cavity, a representation that had already been suggested by Meaburn & Walsh (1980a). It was also shown that the lobes are thin high density sheets of material that can be readily identified as the shocked layers of the cavities. Thus, the combination of a powerful fast wind and a very hard and intense radiation field from the central star, leads to a high degree of excitation throughout NGC 6302. It is probably correct to state that neither one of these sources is negligible at any position, a complicating circumstance when analysing its physical properties. For instance, shock waves will be important not only in the shaping and structuring of the nebula, but also in distorting the emission spectrum from what would be a purely photoionized nebula even in regions where the radiation field is clearly dominant (Peimbert, Sarmiento, & Fierro 1991).

In this work, the analysis of NGC 6302 is taken a step further, inspecting more highly excited gas than in Paper I, with an image centered at [Ne V] 3426 Å. Research around this line has been fruitful, but the data that have been gathered so far do not furnish information on its spatial distribution. Given the specific properties of NGC 6302, this is a valuable addition to the understanding of this object, specially when it is confronted with nebular images of other ions. Also, in order to inspect any possible relation between excitation mechanism and temperature, images in the light of [O III] 4363 and [N II] 5755 Å were obtained and used to produce and compare temperature maps derived from the [N II] $\lambda\lambda$6584/5755 and [O III] $\lambda\lambda$5007/4363 ratios (T[N II] and T[O III]). As was pointed out in Paper I, image calibration suffered from insufficient information on the positions and apertures used in spectroscopic studies. New spectroscopic observations, one of these in a region not studied before, were obtained to address this problem. The paper is organized as follows: the experimental setup is described in § 2, spectroscopic results are presented in § 3, imaging is discussed in § 4, and the main conclusions are given in § 5.

2. OBSERVATIONS AND DATA REDUCTION

2.1. *Spectroscopy*

Spectroscopy was carried out on July 9–12 1997, with the Boller & Chivens spectrograph and the 2.1-m f/7.5 telescope of the Observatorio Astronómico Nacional at San Pedro Mártir, B. C., México. A Tektronix TK1024AB CCD chip was used. The slit was 250 μm wide, aligned in the NS direction. Spectra covering the following overlapping wavelength intervals were obtained: 3200–5270, 4750–6860, 6600–8730 and 8430–10,590 Å. A 600 lines mm^{-1} grating blazed at 4550 Å was used for the blue and green domains, a 600 lines mm^{-1} grating blazed at 6825 Å for the other two. The mean spectral resolution and dispersion are $\sim$ 3 pixel and 2.1 Å/pixel respectively. Short exposures were secured for the first two wavelength intervals (60 and 15 seconds respectively) to avoid saturation of the brightest lines. Longer exposures (10 minutes) were obtained in all ranges to get good quality data in fainter lines. Flux calibration was performed with standard stars HZ 44 and EG 274.

Data reduction was performed using IRAF[2] stan-

[2] IRAF is distributed by NOAO which is operated by AURA under contract to the NSF.

dard procedures. Results are presented in Table 1. These are for a 5″ × 3″ aperture (NS and EW axes respectively). The spectra presented in Table 1 are for the following positions (see Fig. 1*d*): BP is ∼ 1–1.5″ W of the brightness peak of NGC 6302 (source GSC07373–00818 from the Hubble Guide Star Catalogue: $\alpha = 17^h13^m44.56^s$, $\delta = -37°06'11.5''$, epoch = 2000.0), BPS is 7″ south of BP and BPW is 31″ W and 2″ S of BP. Aperture centers are correct within ≤ 1.5″.

Measurement errors are smaller than 10% for line fluxes larger than ∼ 0.05 the Hβ flux at the brightness peak (BP), or 1.5×10^{-12} erg cm^{-2} s^{-1}. Uncertainties can be as large as 50% for the smallest fluxes reported in Table 1 (1.2×10^{-15} erg cm^{-2} s^{-1}). The slit was sufficiently long to extract an adjoining sky background region. Telluric absorption bands are very important beyond ∼ 7000 Å, particularly in low to medium dispersion spectroscopy, and can affect even the brightest source lines. No attempt was made to model and correct for this effect. The four overlapping spectra had to be scaled in order to present all line intensities with respect to Hβ. Scale factors were determined from the strongest lines common to contiguous spectra: Hβ (blue-green), [S II] λλ6717,6731 (green-red) and, for the longest wavelengths, [Cl II] λ8579, Pa14 and Pa13. Scaling errors are between 5 and 10% for region BP, and 10 to 20% for the other two. The smallest errors are for the blue-green overlap. Reddening corrections were performed with Seaton's (1979) extinction law, assuming Hα/Hβ = 2.8 in all cases. Notice that the dereddened ratios for He II λλ4686/10,123 and [S II] λλ4072/10,300 are surprisingly close to theoretical values. Such good agreement is probably fortuitous (*but* comforting) and errors introduced by dereddening can be as large as ∼ 10% in region BP and ∼ 20% in the other two, as can be seen when inspecting the H I and He II recombination series.

2.2. *Imaging*

Images for [O III] λ4363, [O III] λ5007, [N II] λ5755, [N II] λ6584 and a continuum at 5954 Å, were obtained on July 18 and 19 1993, with the same telescope and a Thomson TH31156 1024 × 1024 Metachrome II coated CCD chip. Exposure times were 60 minutes for [O III] λ4363 and [N II] λ5755, 20 minutes for the others. Images for [N II] λ6584 and [Ne V] λ3426 were obtained on August 16 and 17 1996, with the same telescope and the TK1024AB CCD detector. Exposure times were 10 and 40 minutes respectively. The average image quality, measured with the FWHM of stars, was 1.2″ (July 1993) and 1.8″ (August 1996). Sky exposures were secured for flat fields. Most filters were designed for the f/7.5 beam, and an operating temperature of 0°C. The exception is the filter for [Ne V] λ3426, which was designed for a 0° angle of incidence and an operating temperature of 20°C. The minimum bandwidth in these filters is 10 Å. Dome temperature was around 10°C in the 1993 run, nearly 15°C during the 1996 nights. Correspondingly, the transmission curves were shifted between 1.5 and 3 Å (blue and red region) . Thus, though images were not obtained at peak transmission, all emission lines are well within the transmission curves. No other important lines leak into these filters.

Images were linearly rebinned to adjust their plate scale to the one used in Paper I (0.3″/pixel). In order to obtain a better signal for [O III] λλ5007/4363, the source frames were added to those obtained in June 1992 (Paper I). The resulting total integration times for [O III] λ4363 and [O III] λ5007 are 120 and 50 minutes respectively. Since the bandwidth of the filter used for [N II] λ5755 is relatively large, continuum was subtracted with an image taken with the filter centered at 5954 Å. No other continuum image was necessary, since it is relatively unimportant for the other filters (Paper I). Relative accuracy within the line ratio images is always better than 25%. Images were calibrated using the spectral data reported here. Data reduction was carried out with IRAF.

3. SPECTROSCOPIC RESULTS

Data analysis was carried out using Shaw & Dufour's (1996) public domain program. Electron densities and temperatures derived from various ratios are given in Table 2. The S^+ lines are very well defined in the three inspected regions, and ratios are probably precise at the ∼ 5% level. The Cl^{+2} lines are substantially weaker, and ratios are somewhat less accurate. There are uncertainties on the Ar^{+3} ratios since [Ar IV] λ4711 is blended with He I λ4713 and [Ne IV] λ4715. [Ar IV] λλ4711/4740 was calculated assuming that He I λ4713 = 0.1 He I λ4471 (no collisions) and [Ne IV] λλ4715/4725 = 0.62. Notice that densities derived from the S^+ lines are smaller than those obtained from Cl^{+2} and Ar^{+3}. The reason for this is that the critical density of the sulphur lines is smaller, so that lower density regions are being sampled by the [S II] ratio. Thus, in spite of lower errors associated to the sulphur ratio, electron densities derived from the argon lines are more realistic, and will be used from here on.

Given the intensity of the O^{+2} and N^+ lines, temperatures obtained from these ions are very reliable. Taking into account errors arising from the determination of the extinction coefficient, [O III] λλ5007/4363 and [N II] λλ6584/5755 should be accurate at the 10% level. Other ratios reported in Table 2 have larger errors. In particular, [S III] λλ(9069+9530)/6312 suffers from telluric absorption on the redder lines, as evinced when comparing the measured (2.82 at BP, 3.24 at BPS, and 2.16 at BPW) and theoretical (2.5) values for [S III] λλ9530/9069. Temperature diag-

TABLE 1

SPECTROSCOPY: LINE INTENSITIES

ID	BP		BPS		BPW	
	F_λ	I_λ	F_λ	I_λ	F_λ	I_λ
[Ne V] 3426	167.	394.	...	...	...	...
[O II] 3727	20.3	39.1	43.2	97.0	195.	296.
H9	3.56	6.37	5.20	10.7	...	...
[Ne III] 3869	75.9	133.	87.7	175.	126.	180.
H8+He I	10.0	17.3	11.8	23.2	17.2	24.4
Hε+[Ne III] 3968	32.0	52.8	37.8	70.1	49.8	68.5
He I 4026	1.64	2.61	2.29	4.07	2.93	3.94
[S II] 4069	8.41	13.1	9.89	17.1	10.8	14.3
[S II] 4076	2.38	3.69	3.55	6.10	4.26	5.63
Hδ	18.1	27.7	18.3	30.9	19.1	25.0
He II 4200	1.22	1.77	0.86	1.37	...	...
Hγ	32.6	44.8	33.6	49.7	35.2	43.1
[O III] 4363	30.2	41.0	25.7	37.5	23.4	28.4
He I 4471	3.78	4.78	5.16	6.89	6.19	7.18
He II 4541	2.09	2.52	1.49	1.88	1.58	1.78
[Fe III] 4606	0.64	0.74	0.58	0.70	...	...
N III 4634	3.12	3.56	2.62	3.08	...	...
N III 4641	5.08	5.79	3.37	3.96	1.81	1.97
He II 4686	68.5	75.8	47.9	54.3	40.3	43.0
[Ar IV] 4711 + He I 4713 + [Ne IV] 4715	14.5	15.8	10.3	11.5	8.92	9.44
[Ne IV] 4725	3.53	3.77	2.31	2.51	0.95	0.99
[Ar IV] 4740	21.2	22.7	13.3	14.4	6.76	7.05
Hβ	100.	100.	100.	100.	100.	100.
He I 4922	1.11	1.07	1.76	1.68	...	...
[O III] 4959	467.	441.	438.	408.	432.	417.
[O III] 5007	1446.	1330.	1378.	1243.	1315.	1247.
Si II 5041	1.79	1.60	2.26	1.97	...	...
Si II 5056	0.69	0.62	1.37	1.19	...	...
[N I] 5200	11.4	9.50	23.4	18.7	94.0	83.7
[Fe II] 5261	...	...	0.67	0.51	...	...
[Fe III] 5270	...	...	0.65	0.50	...	...
[Ca V] 5309	0.36	0.28	...	...	...	...
[Cl IV] 5323	0.24	0.19	...	...	...	...
He II 5411	10.0	7.55	7.21	5.10	5.38	4.50
[Cl III] 5518	0.56	0.40	0.93	0.61	1.75	1.41
[Cl III] 5538	1.35	0.95	1.63	1.06	1.62	1.30
[Fe VI] 5677	0.33	0.21	...	...	...	...
[Fe VII] 5721	0.56	0.36	-0.32	0.18	...	...
[N II] 5755	31.8	19.9	40.9	22.9	52.8	39.2
He I 5876	29.1	17.1	40.5	21.0	31.4	22.4
[Fe VII] + [Ca V] 6087	1.00	0.55	0.82	0.39	1.28	0.87
[K IV] 6102	1.71	0.91	1.32	0.61	...	...
[K VI] 6228	0.53	0.27	0.56	0.24	...	...
He II 6234	0.53	0.27	0.49	0.21	...	...
[O I] 6300	41.8	20.7	71.1	29.9	100.	64.0
[S III] 6312	11.6	5.72	15.0	6.27	12.0	7.66
Si II 6347	0.73	0.36	1.37	0.56	...	...
[O I] 6364	14.1	6.83	24.8	10.1	35.1	22.2
Si II 6372	1.17	0.57	1.42	0.58	...	...
He II 6406	0.88	0.42	0.87	0.35	0.70	0.44
[Ar V] 6435	12.2	5.83	9.35	3.76	1.94	1.21

TABLE 1 (CONTINUED)

ID	BP		BPS		BPW	
	F_λ	I_λ	F_λ	I_λ	F_λ	I_λ
[N II] 6548	303.	137.	628.	237.	998.	604.
Hα	622.	280.	748.	280.	465.	280.
[N II] 6584	951.	427.	2021.	753.	sat	...
He I 6678	10.2	4.44	16.7	5.98	10.1	5.95
[S II] 6717	20.5	8.81	57.2	20.2	123.	71.9
[S II] 6731	42.1	18.0	109.	38.2	156.	90.9
He II 6891	1.35	0.55	1.32	0.44	...	...
[Ar V] 7006	26.8	10.6	19.3	6.14	...	...
He I 7065	24.2	9.42	33.0	10.3	14.5	7.96
[Ar III] 7136	75.6	28.9	102.	31.1	82.1	44.5
[Fe II] 7155	0.23	0.09	5.16	1.57	...	...
[Ar IV] 7171	4.30	1.64	4.15	1.26	...	...
He II 7178	2.27	0.86	1.74	0.53	...	...
[Ar IV] 7237	3.35	1.24	3.16	0.93	...	...
[Ar IV] 7263	3.61	1.33	2.45	0.72	...	...
He I 7282	2.88	1.06	3.98	1.16	...	...
[O II] 7320	26.1	9.50	36.7	10.6	27.8	14.6
[O II] 7331	22.9	8.32	30.2	8.66	22.7	11.9
[Ni II] 7378	...	...	3.36	0.95	...	...
[Fe II] 7452	...	...	1.85	0.51	...	...
[Cl IV] 7530	2.76	0.96	1.92	0.52	...	...
He II 7593	4.70	1.60	3.84	1.01	...	...
[Ar III] 7751	21.7	7.14	28.4	7.21	29.8	14.1
[Cl IV] 8046	6.75	2.08	5.09	1.19	...	...
He II 8236	7.12	2.09	5.28	1.17	2.82	1.30
Pa15 8545	2.10	0.56	2.86	0.56	1.23	0.53
[Cl II] 8579	2.38	0.62	3.70	0.71	2.52	1.08
Pa14 8598	2.29	0.59	2.62	0.49	1.16	0.49
[Fe II] 8616	...	...	5.30	0.99	...	...
Pa13 8665	3.40	0.86	3.32	0.61	2.74	1.14
Pa12 8750	3.60	0.89	4.03	0.72	1.59	0.65
Pa11 8863	5.06	1.22	6.57	1.14	...	...
Pa10 9015	6.88	1.58	6.28	1.02	3.11	1.22
[S III] 9069	188.	41.9	210.	33.0	132.	51.
[Cl II] 9123	0.88	0.19	1.54	0.24	...	...
Pa9 9228	10.8	2.34	11.7	1.78	5.98	2.26
[S III] 9531+Pa8	550.	118.	715.	107.	292.	110.
He II 9761	1.07	0.23	...	...	...	...
[C I] 9850	1.25	0.27	...	...	...	...
9872	1.16	0.25	9.66	1.43	...	...
[S VIII] 9913	5.81	1.23	12.9	1.91	...	...
Pa7 10,049	22.2	4.68	31.7	4.64	15.2	5.63
He II 10,123	97.6	20.5	100.	14.6	31.9	11.8
[S II] 10,287	17.2	3.58	56.8	8.19	...	...
[S II] 10,321	17.4	3.62	22.7	3.27	...	...
[S II] 10,337	12.5	2.60	14.8	2.13	...	...
[S II] 10,371	8.85	1.84	...	...	...	...
[N I] 10,398	27.3	5.66	...	...	...	...
[N I] 10,408	19.3	4.00	...	...	...	...
$F(H\beta)$ (erg cm^{-2} s^{-1})	2.92×10^{-12}		6.15×10^{-13}		1.68×10^{-13}	
$c(H\beta)$	1.07		1.32		0.68	
$I(H\beta)$ (erg cm^{-2} s^{-1})	3.43×10^{-11}		1.28×10^{-11}		8.04×10^{-13}	

TABLE 2

SPECTROSCOPY: DENSITY AND TEMPERATURE

	BP Ratio	N_e (10^4 cm^{-3})	BPS Ratio	N_e (10^4 cm^{-3})	BPW Ratio	N_e (10^4 cm^{-3})
[S II] 6717/6731	0.49±0.02	$1.28^{+0.60}_{-0.34}$	0.53±0.03	$0.72^{+0.32}_{-0.17}$	0.79±0.04	$0.14^{+0.03}_{-0.02}$
[Cl III] 5518/5538	0.42±0.04	$1.86^{+0.48}_{-0.35}$	0.58±0.06	$0.87^{+0.24}_{-0.17}$	1.08±0.11	$0.15^{+0.07}_{-0.06}$
[Ar IV] 4711/4740	0.57±0.09	$1.63^{+0.71}_{-0.36}$	0.64±0.09	$1.34^{+0.23}_{-0.33}$	1.15±0.18	$0.20^{+0.27}_{-0.14}$
	Ratio	T_e (10^4 K)	Ratio	T_e (10^4 K)	Ratio	T_e (10^4 K)
[Cl IV] (8046+7530)/5323	16.0±2.40	$1.75^{+indef}_{-0.18}$	...	...	...	...
[O III] (5007+4959)/4363	43.2±4.32	$1.84^{+0.14}_{-0.12}$	44.0±4.40	$1.84^{+0.13}_{-0.10}$	58.6±5.86	$1.61^{+0.09}_{-0.08}$
[S III] (9069+9530)/6312	28.0±5.60	$1.47^{+0.26}_{-0.17}$	22.3±4.46	$1.74^{+0.41}_{-0.21}$	21.0±4.20	$1.88^{+0.46}_{-0.24}$
[N II] (6584+6548)/5755	28.3±2.83	$1.48^{+0.18}_{-0.17}$	43.2±4.32	$1.19^{+0.10}_{-0.10}$	60.8±6.08	$1.13^{+0.07}_{-0.04}$

nostics from S^+ and O^+ were not considered since the lines involved in the ratios ([S II] $\lambda\lambda$6724/4070 and [O II] $\lambda\lambda$3727/7325) are produced in very different regions since their critical densities differ greatly (Mathis, Torres-Peimbert, & Peimbert 1998): $\sim 10^4$ cm^{-3} for [S II] λ6724 and [O II] λ3727, $> 10^6$ cm^{-3} for [S II] λ4070 and [O II] λ7325.

The temperature derived from the O^{+2} lines is very similar to the one found by Oliva et al. (1996). On the other hand, McKenna et al. (1996) give a temperature of 12,180 K using the spectroscopic data of Aller & Czysak (1978). Differences in reddening corrections and the measured flux for [O III] λ5007 may account for this discrepancy. A fair agreement among these works exists for temperatures derived from N^+ (between 14,100 and 14,800 K).

Ion concentrations are presented in Table 3. The determination of ion abundances is highly dependent on the temperature, and errors were calculated from the temperature range. Concentrations are usually determined with $T(N^+)$ for neutrals and low ionization species, and $T(O^{+2})$ for all others. Kingsburgh & Barlow (1994) modify this scheme, adjusting the temperatures to the ionization potentials. For instance, a temperature intermediate between $T(N^+)$ and $T(O^{+2})$ is used when calculating the abundance of S^{+2}. More recently Peimbert, Luridiana, & Torres-Peimbert (1995) used $T(C^{+2})$ to determine the concentration of He^+ and O^{+2}. With this temperature they find nearly equal He^+ abundances when various He I lines are used. But this assumption leads to the implausible situation where, for instance, the abundance of O^+ is determined from a higher temperature than the one used for O^{+2}, since in many cases it happens that $T(N^+) > T(C^{+2})$. A modified version of the Kingsburgh & Barlow (1994) scheme is adopted here: the temperatures used to calculate all ion concentrations, not only that of S^{+2}, are adjusted to the ionization potentials following the prescription given by these authors. Thus, ion concentrations are determined from the following temperatures: O^0, N^0, N^+, O^+, S^+ and Cl^+ with $T(N^+)$; He^+, S^{+2}, Ar^{+2}, Cl^{+2} with $T(N^+) + [T(O^{+2}) - T(N^+)]/3$; He^{+2}, Ne^{+2}, Ar^{+3}, Cl^{+3} and K^{+3} with $T(O^{+2})$; Ar^{+4} and Ne^{+3} with $T(O^{+2}) + 1000$; and Ne^{+4} with $T(O^{+2}) + 2270$.

There has been some dispute regarding the temperature of the region where Ne^{+4} is prevalent. From the [Ne V] λ14.3 μm/3426 Å ratio, Rowlands et al. (1994) determined an electron temperature $\sim$ 70,000 K with $c(H\beta) = 1.59$. This high temperature has been recently questioned. Oliva et al. (1996) point out that the value assumed for the extinction is too large, and also suggest that such a high temperature rather indicates that the ground state collision strengths for this ion are overestimated by a factor $\sim$ 3. Using new ISO data and a smaller extinction coefficient, Pottasch et al. (1996) recalculated the temperature and the density, and found that T_e = 21,000 K and N_e = 18,000 cm^{-3} without having to invoke different atomic parameters for Ne^{+4}. These values are nearly identical to those assumed here.

The abundance of helium ions was determined following Aller (1984). Collisional effects at the densities and temperatures prevalent in these regions are very large for the He I lines, and were taken into account to find the He^+ abundance (Kingdon & Ferland 1995). The substantial range in temperatures and densities was considered when calculating errors in the He^+ abundance. All other ion abundances were determined following Shaw & Dufour (1996).

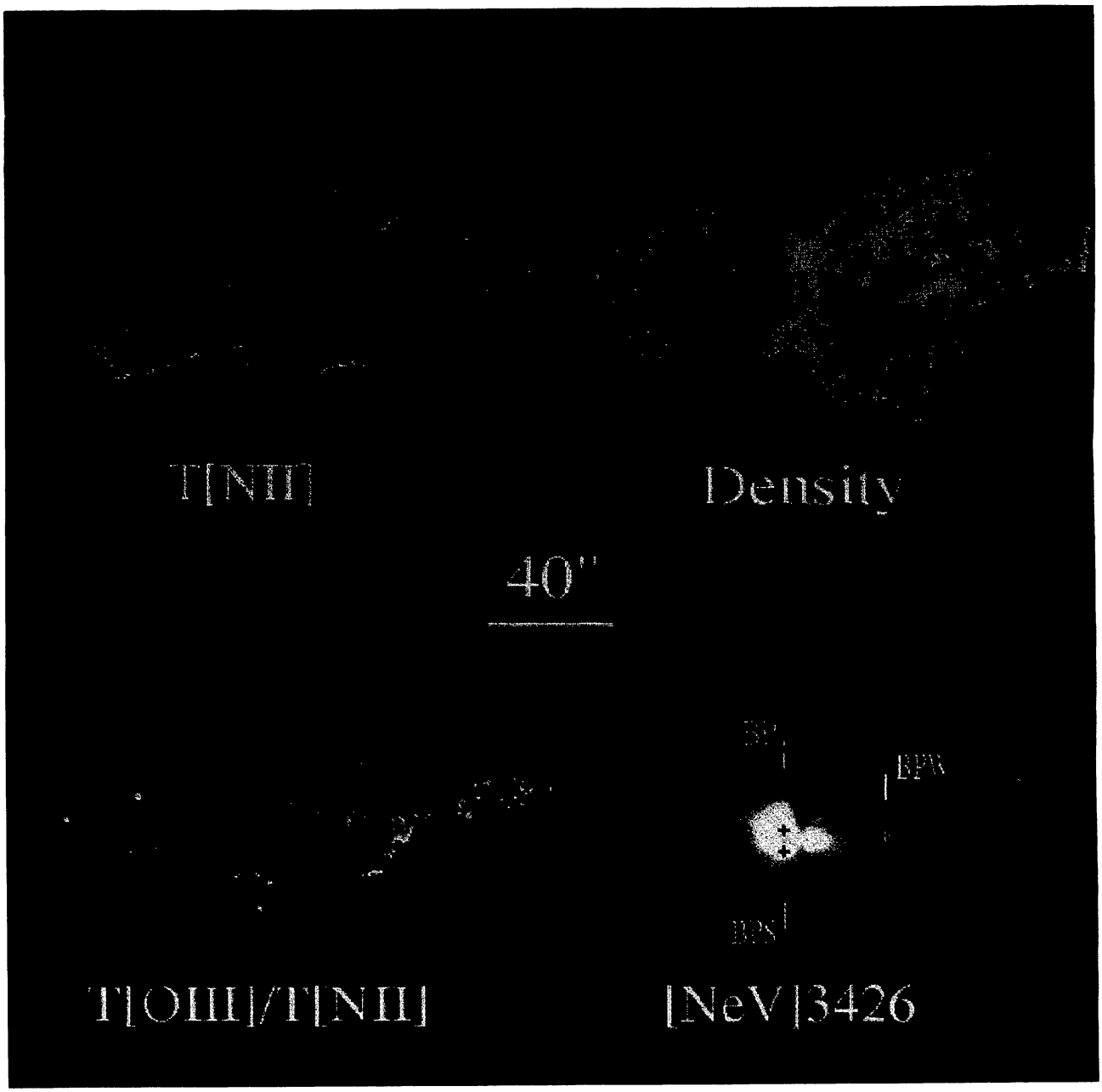

Fig. 1*(a)*. Nitrogen temperature 5000 – 20,000 K, *(b)* Density, 2 – 5 cm^{-3} (logarithmic scale), *(c)* T[O III]/T[N II] (0.9 – 2.3), and *(d)* [Ne V] λ3426 (0 – 1.6 in arbitrary units, logarithmic scale) images. The largest values are represented in white in all cases. Spectroscopically observed positions are marked in Figure 1*d*.

Fig. 5. Image of [Ne V] λ3426/Hβ. The image range is 0 – 3.45. The largest values are represented in white.

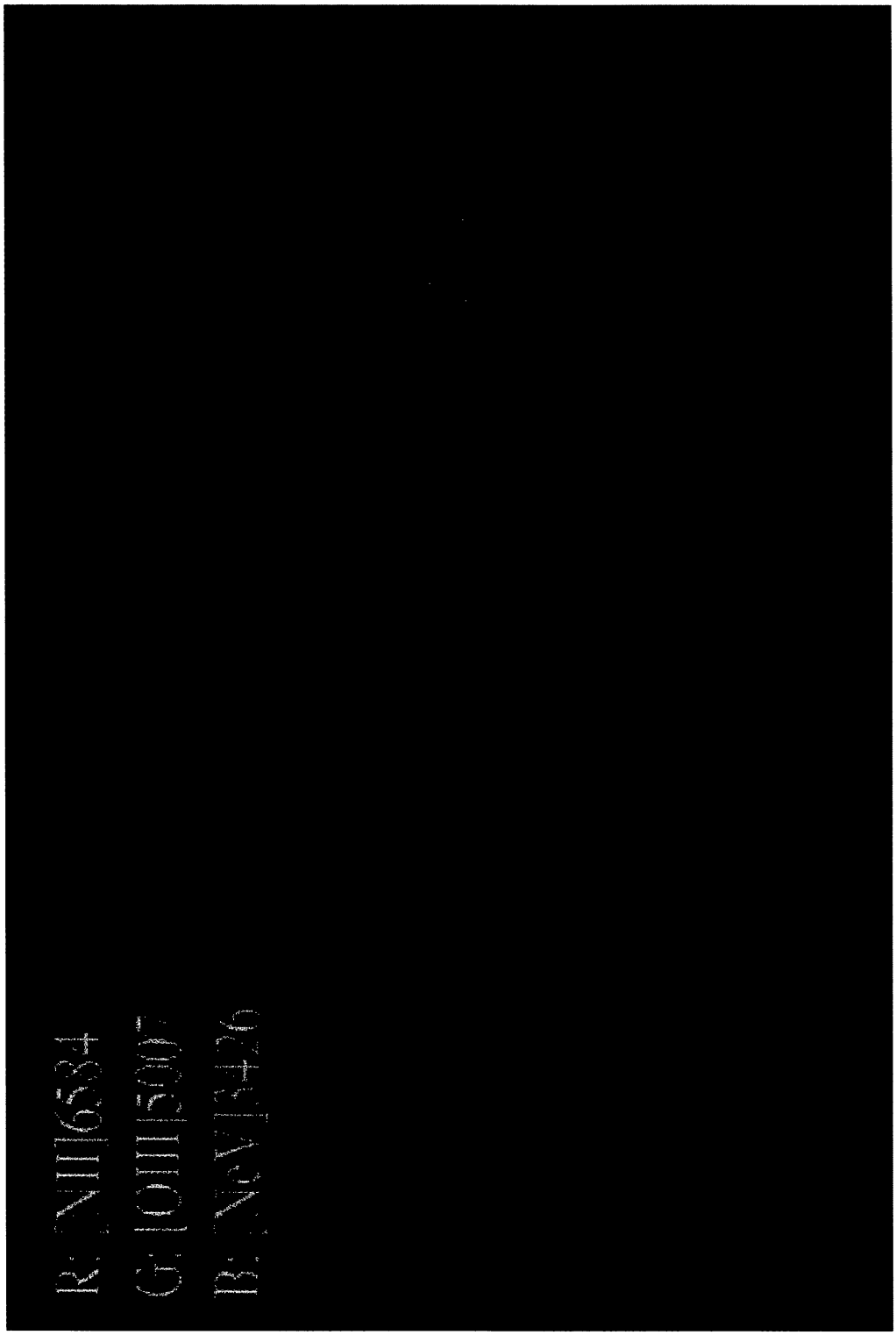

Fig. 7. RGB image of [N II] λ6584 (r), [O III] λ5007 (g), and [Ne V] λ3426 (b).

TABLE 3

SPECTROSCOPY: ION ABUNDANCES

Ion		Lines	BP	BPS	BPW
He^{+}		4471	$0.090\ ^{+0.011}_{-0.010}$	$0.146\ ^{+0.011}_{-0.009}$	$0.178\ ^{+0.012}_{-0.013}$
...		5876	$0.084\ ^{+0.009}_{-0.008}$	$0.114\ ^{+0.008}_{-0.006}$	$0.148\ ^{+0.015}_{-0.014}$
...		6678	$0.104\ ^{+0.002}_{-0.003}$	$0.143\ ^{+0.003}_{-0.002}$	$0.153\ ^{+0.006}_{-0.005}$
He^{+2}		4686	0.082	0.058	0.047
O^{0}	($\times10^{-5}$)	6300	$1.18\ ^{+0.53}_{-0.32}$	$3.36\ ^{+1.17}_{-0.78}$	$8.52\ ^{+1.15}_{-1.56}$
O^{+}	($\times10^{-5}$)	3726,3729	$1.15\ ^{+0.57}_{-0.33}$	$5.34\ ^{+2.22}_{-1.39}$	$9.06\ ^{+4.24}_{-2.47}$
O^{+}	($\times10^{-5}$)	7320,7330	$1.51\ ^{+1.05}_{-0.53}$	$4.59\ ^{+2.71}_{-1.50}$	$14.7\ ^{+10.1}_{-5.20}$
O^{+2}	($\times10^{-5}$)	5007	$9.37\ ^{+1.53}_{-1.34}$	$8.73\ ^{+1.16}_{-1.17}$	$11.8\ ^{+1.50}_{-1.50}$
N^{0}	($\times10^{-5}$)	5200	$1.08\ ^{+0.39}_{-0.24}$	$3.20\ ^{+0.99}_{-0.66}$	$4.66\ ^{+1.81}_{-0.84}$
N^{+}	($\times10^{-4}$)	6584	$0.40\ ^{+0.12}_{-0.08}$	$1.09\ ^{+0.26}_{-0.19}$	$2.58\ ^{+0.24}_{-0.34}$
S^{+}	($\times10^{-6}$)	6716,6731	$1.01\ ^{+0.26}_{-0.18}$	$2.93\ ^{+0.64}_{-0.46}$	$3.64\ ^{+0.32}_{-0.45}$
S^{+}	($\times10^{-6}$)	4068,4076	$0.77\ ^{+0.27}_{-0.18}$	$1.96\ ^{+0.62}_{-0.41}$	$3.32\ ^{+0.44}_{-0.59}$
S^{+2}	($\times10^{-6}$)	6312	$2.36\ ^{+0.88}_{-0.55}$	$3.82\ ^{+1.05}_{-0.79}$	$6.58\ ^{+1.00}_{-1.21}$
Ne^{+2}	($\times10^{-5}$)	3869	$1.59\ ^{+0.28}_{-0.24}$	$2.09\ ^{+0.30}_{-0.30}$	$3.04\ ^{+0.45}_{-0.40}$
Ne^{+3}	($\times10^{-5}$)	4725	$2.21\ ^{+0.83}_{-0.62}$	$1.53\ ^{+0.46}_{-0.42}$	$1.55\ ^{+0.48}_{-0.38}$
Ne^{+4}	($\times10^{-5}$)	3426	$3.79\ ^{+0.65}_{-0.60}$	...	...
Ar^{+2}	($\times10^{-6}$)	7751	$1.06\ ^{+0.22}_{-0.15}$	$1.34\ ^{+0.20}_{-0.17}$	$3.11\ ^{+0.33}_{-0.26}$
Ar^{+3}	($\times10^{-7}$)	4740	$9.03\ ^{+1.21}_{-1.16}$	$5.84\ ^{+0.68}_{-0.76}$	$4.48\ ^{+0.48}_{-0.45}$
Ar^{+4}	($\times10^{-7}$)	7006	$5.09\ ^{+0.58}_{-0.59}$	$2.95\ ^{+0.28}_{-0.32}$	...
Cl^{+}	($\times10^{-8}$)	8579	$3.03\ ^{+0.62}_{-0.45}$	$4.91\ ^{+0.82}_{-0.63}$	$8.16\ ^{+0.56}_{-0.81}$
Cl^{+2}	($\times10^{-8}$)	5518,5538	$3.64\ ^{+0.91}_{-0.60}$	$5.63\ ^{+1.05}_{-0.85}$	$8.85\ ^{+0.98}_{-1.19}$
Cl^{+3}	($\times10^{-8}$)	8046	$5.50\ ^{+0.71}_{-0.65}$	$3.15\ ^{+0.32}_{-0.35}$	...
K^{+3}	($\times10^{-8}$)	6102	$6.68\ ^{+0.82}_{-0.75}$	$4.48\ ^{+0.46}_{-0.47}$	...

Elemental abundances are presented in Table 4. Helium abundance is for the He^{+} concentration determined from He I λ6678, and not the brighter He I λ5876 line as is usually the case. This choice is based on the fact that collisional corrections for He I λ6678 are some 3 times smaller, leading to a better estimate of the He^{+} concentration in this very dense and hot medium. Furthermore, differences between the total helium abundance at the three observed positions are significantly smaller when this line is used. Ion concentrations were added when calculating the abundance of Ne and Cl. The abundance of O, N, S, and Ar was determined from the "standard" ICF's (equations A1, A9, A30, and A36) given by Kingsburgh & Barlow (1994), with the He^{+} abundance derived from He I λ6678. The concentration used for O^{+} is the one inferred from [O II] $\lambda\lambda$7320,7330 since these lines have a higher critical density. For the same reason, the [S II] $\lambda\lambda$4068,4076 lines were considered as leading to a better estimate of the S^{+} abundance.

When comparing total abundances in the three inspected regions, it stands out that these can be 2 to 3 times larger in region BPW. Conditions at this position, which is some 30″ away from BP ($\sim$ 0.3 pc at a distance of 2 kpc), are substantially milder in all respects. In particular, the relative abundance of all ions (Table 3) imply that higher ionization stages are considerably less populated (though not absent, since imaging indicates that [Ne V] λ3426/Hβ $\simeq$ 0.57 at this position). It is then expected that errors introduced by the ICF's will be less conspicuous, and calculated abundances will be closer to reality.

This is substantiated when these results are compared to those obtained by Aller et al. (1981) (henceforth ARMK), who calculated the elemental abundances in NGC 6302 (at or close to position BP) using data from the *IUE*, thus having access to highly

TABLE 4

SPECTROSCOPY: ABUNDANCES

Element		BP	BPS	BPW	ARMK
He	...	$0.186\ ^{+0.002}_{-0.003}$	$0.201\ ^{+0.003}_{-0.002}$	$0.200\ ^{+0.006}_{-0.005}$	0.18
O	($\times 10^{-4}$)	$1.60\ ^{+0.40}_{-0.28}$	$1.67\ ^{+0.49}_{-0.34}$	$3.17\ ^{+1.41}_{-0.82}$	2.95
N	($\times 10^{-4}$)	$4.24\ ^{+2.76}_{-1.74}$	$3.97\ ^{+1.84}_{-1.31}$	$5.56\ ^{+1.42}_{-1.42}$	5.90
Ne	($\times 10^{-5}$)	$7.59\ ^{+1.75}_{-2.02}$	$> 3.75\ ^{+0.81}_{-0.74}$	$> 4.53\ ^{+0.94}_{-0.78}$	8.96
S	($\times 10^{-6}$)	$4.92\ ^{+2.32}_{-1.47}$	$6.78\ ^{+2.33}_{-1.65}$	$10.5\ ^{+1.80}_{-2.09}$	2.16
Ar	($\times 10^{-6}$)	$2.73\ ^{+0.56}_{-0.41}$	$3.06\ ^{+0.74}_{-0.53}$	$6.63\ ^{+1.95}_{-1.17}$	5.22
Cl	($\times 10^{-7}$)	$1.16\ ^{+0.16}_{-0.14}$	$1.22\ ^{+0.15}_{-0.13}$	$> 1.68\ ^{+0.18}_{-0.17}$	...

ionized species of nitrogen and oxygen. ARMK give the sum of all ionic species as well as a determination of elemental abundances based on ICF's normally used when only a few ionization stages are observed. These unexplained corrections may be objectionable, so the comparison is carried out with their sum of ion concentrations, also included in Table 4. Notice that the elemental abundances of oxygen and nitrogen at BPW are quite similar to the sum of ions given by ARMK. It must be pointed out that their ion abundances were calculated assuming different temperatures and using older physics. Recalculating the oxygen abundance with the temperatures and physics used here, smaller values are derived (2.36×10^{-4} versus 2.95×10^{-4} in ARMK), but still larger than those determined from the ICF's.

Thus, "standard" ICF's underestimate the abundance of higher ionization stages at and around the brightest and very highly excited region in NGC 6302. The discrepancy in region BP may be larger, since even more highly ionized species (unobserved by the *IUE*) may be present. Taking as a conservative reference the detection of Ne^{+4} and Ne^{+5} (Pottasch et al. 1986), up to O^{+5}, N^{+6}, S^{+6} and Ar^{+7} may be expected. Notice that still more highly ionized species have been observed, such as Si^{+6} (Ashley & Hyland 1988), Mg^{+7} (Pottasch et al. 1996), and S^{+7} (Reconditi & Oliva 1993; this paper), though the existence of at least one of these may be difficult to explain with pure photoionization models (280.9 eV photons are required to produce S^{+7}).

Taking advantage of the fact that neon has been observed up to the fourth ionization stage at position BP, oxygen abundance can also be calculated using the ICF recommended for very highly excited regions, i.e., those where all He is found in the doubly ionized state (equation A39 in Kingsburgh & Barlow 1994). This ICF is also used for argon. The "standard" ICF's are used for the other elements. In this case the derived abundances are: $5.2\ ^{+1.5}_{-1.5} \times 10^{-4}$ for oxygen, $13.7\ ^{+6.0}_{-5.3} \times 10^{-4}$ for nitrogen, $6.9\ ^{+3.5}_{-2.4} \times 10^{-6}$ for sulphur and $4.3\ ^{+0.8}_{-1.1} \times 10^{-6}$ for argon. Though the abundance of oxygen seems to be closer to reality given the above discussion, bear in mind that He^{+2} is far from being the predominant helium ion in region BP.

In conclusion, the real abundance of neon is at least equal to the sum of ion concentrations in region BP, those for chlorine, sulphur and argon are likely to be close to their values at position BPW, whereas those for oxygen and nitrogen, may be intermediate between those determined in region BPW with the "standard" ICF's and those found in region BP using the ICF for highly excited regions. But take notice that all forbidden lines in the spectrum at BPW are very intense in comparison with the hydrogen recombination lines (for instance, Hα/[S II] λ6724 = 1.72), which is one of the most significant features of shock excited regions.

4. IMAGING

4.1. *T[O III] and T[N II]*

The oxygen and nitrogen temperature maps (T[O III] and T[N II]) were determined from the [O III] $\lambda\lambda$5007/4363 and [N II] $\lambda\lambda$6584/5755 images, using the following formulae (McKenna et al. 1996)

$$T[\mathrm{N\ II}] = \frac{10697.5}{\log(R_{\mathrm{N\ II}}) - 0.888527 + \log(1 + 0.310077x)} \quad (1)$$

and

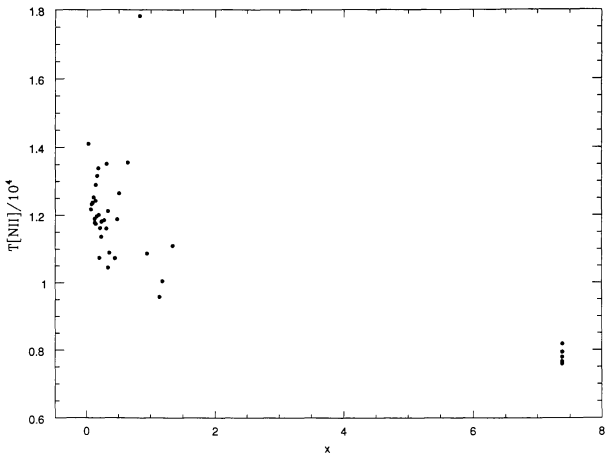

Fig. 2. x versus T[N II].

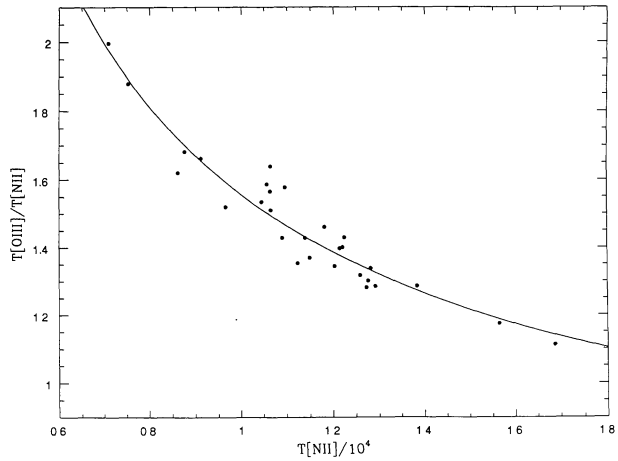

Fig. 3. T[O III]/T[N II] versus T[N II].

$$T[\mathrm{O\ III}] = \frac{14516.0}{\log(R_{\mathrm{O\ III}}) - 0.871411 + \log(1 + 0.046874x)} \quad ; \quad (2)$$

where $R_{\mathrm{N\ II}} = (\lambda\lambda 6548{+}6584)/5755$, $R_{\mathrm{O\ III}} = (\lambda\lambda 4959{+}5007)/4363$, and $x = (N_e/10^2)T^{-1/2}$. These formulae are accurate approximations for a wide range in temperatures and densities (T_e = 5000 – 20,000 K and $N_e = 10^4 - 10^6$ cm^{-3}). The x parameter image was obtained in Paper I.

The nitrogen temperature map is displayed in Figure 1*a* (Plate 1). In the mean, T[N II] is some 1500 K larger in the eastern lobe ($\sim$ 11,800±1100 versus 10,300±1600). Likewise, T[O III] is about 800 K larger ($\sim$ 17,000±800 versus 16,200±1500). This was already pointed out in Paper I when analyzing the T[O III] map, where it was suggested that the western lobe is colder because its higher mean density leads to more efficient cooling. This is confirmed, globally and locally, when the density (Figure 1*b*, Plate 1) and T[N II] maps are confronted. A plot of x versus T[N II] with 41 randomly selected pointings in the nebula, 2″ × 2″ each, renders additional support to this hypothesis (Figure 2): T[N II] is markedly smaller once $x \geq 1$. There is no apparent relation between density and temperature when x is smaller, i.e., a range of temperatures can be found for any given value of $x < 1$.

The oxygen to nitrogen temperature ratio, T[O III]/T[N II], is displayed in Figure 1*c* (Plate 1). T[O III] is everywhere greater than T[N II]. The ratio attains its smallest value at position BP ($\sim$ 1), and is close to 2 in several regions. With one exception (near the center of the western lobe), these are high density regions. There is a surprisingly tight correlation between T[N II] and T[O III]/T[N II], as evinced in Figure 3, where 30 randomly selected regions (2″ × 2″ each) distributed over the entire T[O III]/T[N II] map are plotted. An excellent fit (also plotted in this figure) is obtained with

$$T[\mathrm{O\ III}]/T[\mathrm{N\ II}] = 0.536 + 1.022/t[\mathrm{N\ II}] \ , \quad (3)$$

where t[N II] = T[N II]/10^4. The typical error is 0.057 and the correlation coefficient is 0.955. Thus, the O^{+2} and N^+ regions are more segregated in less excited regions. Since cooling in a uniform density medium is more efficient in the O^{+2} zone (Stasinska 1980; Shaver et al. 1983), this apparently implies that the less highly excited regions in NGC 6302 are much denser. Moreover, equation (3) would indicate that differences are more pronounced in higher density regions. But it is difficult to understand why this occurs in the manner prescribed by this equation.

An additional point of interest was to search for any possible temperature or density signature in regions defined as shock excited based on the [S II] λ6724/Hα line ratio (Paper I). Nothing conspicuous was found in relation to T[O III] or T[O III]/T[N II], though these images are rather limited in extent. The nitrogen temperature map is much more extended, but still no systematic connection between T[N II] and shock excitation could be found. The same applies for the density: large and small values of [S II] λ6724/Hα (shock excited and photoionized gas) can be indistinctly found in dense and rarefied media.

This seems rather surprising since, among other things, shocks are an additional heat source. If shocks are indeed present in NGC 6302, the absence of any observable temperature signature may indi-

cate that post-shock cooling occurs very quickly and over a small distance. The cooling time, t_{cool}, is defined as

$$t_{cool} = \frac{m_i V_s^2}{2n\Lambda(T_s)} , \quad (4)$$

where m_i is the mean particle mass, V_s the shock velocity, n the post-shock density and $\Lambda(T_s)$ the cooling function at the post-shock temperature T_s. Since $T_s \simeq 1.5 \times 10^5\ V_7^2$ K (V_7 is the shock velocity in 100 km s^{-1}) and the cooling function (see Raymond, Cox, & Smith 1976) is $\simeq 10^{-19}\ T_s^{-1/2}$ erg cm^3 s^{-1} for $T_s \simeq 1 - 500 \times 10^5$ K ($V_7 \simeq 0.8$–18), it follows that

$$t_{cool} \simeq 1.2 \times 10^4\ V_7/n \ \text{ yr} . \quad (5)$$

For $V_7 = 1 - 4$ and $n = 10^3 - 10^4$ cm^{-3}, cooling occurs very quickly (1 – 50 yr) and over a small distance (0.01 – 0.0001 pc, or 1 – 0.01″ at 2 kpc). This distance scale is under the resolution of these images and the transition happens so rapidly that it is doubtful that the ionization state of the plasma would change during the shock transition. The main effect of this isothermal shock is to compress the gas by a factor of M^2 (M is the Mach number) at the most (magnetic pressure will inhibit compression). All things being equal, cooling should be more efficient here, and lower ionization stages should become more abundant (as in region BPW). And yet, there is no clear indication that low ionization species are more abundant when density gradients are large. Serious theoretical research is clearly required to address this question.

4.2. *The [Ne V] Image*

A flux calibrated image of NGC 6302 in the light of [Ne V] λ3426 is displayed in Figure 1*d* (Plate 1). This is probably the first Ne^{+4} image of a planetary nebula. A scan accross the EW axis of this image is presented in Figure 4. Line brightness falls 300 times some 38″E and 52″W from position BP. The detection limit is about twice as small (5.5×10^{-16} erg cm^{-2} s^{-1} for a 1″ × 1″ aperture). No conspicuous feature of NGC 6302 can be readily identified from this image. This information is conveyed, as is usually the case, when it is compared with some other line. A [Ne V] λ3426/Hβ extinction corrected image is shown in Figure 5 (Plate 2) (the Hβ frame is from Paper I). Several interesting and novel features stand out from this image.

The lane bisecting the nebula is nowhere as evident as in this frame. The relative position of the high excitation peaks at each side of the lane is particularly interesting, since it provides information on

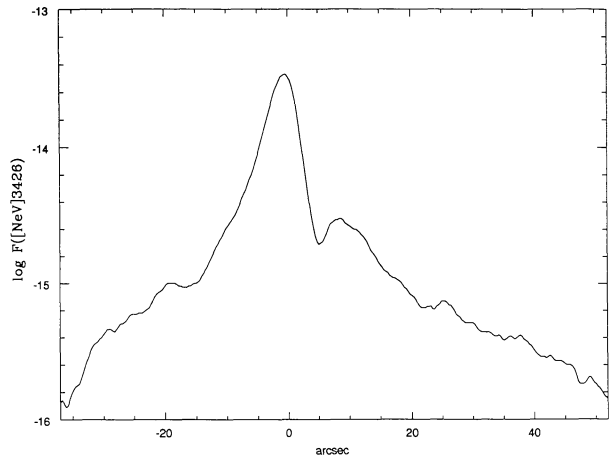

Fig. 4. Scan accross the equatorial plane of log F([Ne V] λ3426), centered at position BP (at 0″).

the geometrical disposition of the toroid of material blocking the outflow of gas and radiation from the central star (Rodríguez et al. 1985), as well as on the inclination of the nebula with respect to the line of sight. Crude measurements lead to a PA $\sim -25°$ for the toroid, and an inclination angle of 50° with respect to the line of sight for the nebula, with the western lobe on the far side. The latter is nearly identical to the inclination angle reported for the toroid (Rodríguez et al. 1985).

Beyond both peaks, and along the equatorial plane, the highly excited plasma extends in a manner not unlike the way that gas expands beyond a jet nozzle. This is the radiatively ionized high velocity wind identified by Meaburn & Walsh (1980a) in profiles of the [Ne V] λ3426 Å line. The degree of excitation initially lessens away from the equatorial plane, but the gas is then "re-excited" in four arches, those to the east very well defined, conforming a bipolar structure. A scan perpendicular to the equatorial plane (Figure 6), centered 8″ E from BP, shows the magnitude of this "re-excitation". Two of these arches (NE and SW) are located between the low excitation filaments that were interpreted in Paper I as shock excited, based on the Hα/[S II] λ6724 ratio (≤ 2). The other two (NW and SE) lie beyond the corresponding outermost low excitation filament. A possible explanation for these arches is that highly excited gas is being funneled along these directions by a physical constraint. An alternative interpretation is that the gas is truly being decelerated and re-excited as it collides with the walls of the bipolar cavity. Given the very large velocity of this gas, this would not be surprising, but the comparison with

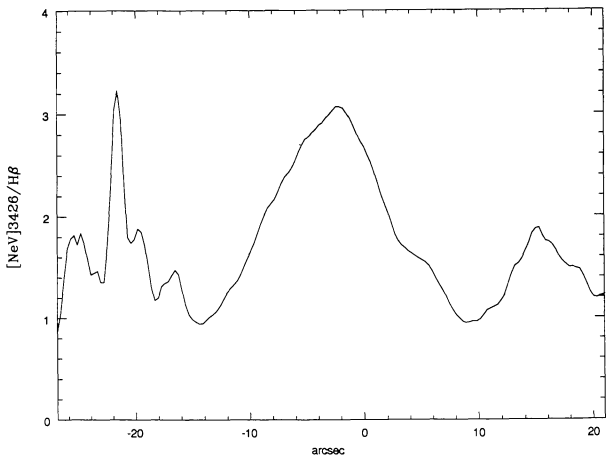

Fig. 6. Scan perpendicular to the equatorial plane of [Ne V] λ3426/Hβ, centered 8″ E from position BP (at 0″).

the low excitation shock excited filaments does not support conclusively this alternative. A kinematical analysis could settle this question.

Images of [N II] λ6584 (R), [O III] λ5007 (G), and [Ne V] λ3426 (B) are combined in the RGB frame presented in Figure 7 (Plate 3). Given the large difference of energies required to produce N^+ (14.5 eV), O^{+2} (35.1 eV) and Ne^{+4} (97.1 eV), this is probably the best depiction of the excitation level of the entire nebula that can be obtained from optical data alone. The northern part of the bisecting lane is clearly dominated by [O III] λ5007 emission, whereas the highly excited gas is mostly found in the equatorial plane. As mentioned, the high and low excitation arches do not coincide, and there is no uniform pattern as to their relative distribution. Low excitation prevails in isolated regions located towards the periphery. The most conspicuous and extensive lies to the west, in a dense medium dominated by shocks (Paper I). This region is relatively close to the position where King, Scarrott, & Shirt (1985) suggest that there may be an illuminating star and Meaburn & Walsh (1980b) propose that there could be a secondary wind source. The low excitation level prevailing in this region does not support the idea of an additional energy source.

5. CONCLUSIONS

1. Care should be taken when using ICF's in the most highly excited regions of NGC 6302. The "standard" ICF's given by Kingsburgh & Barlow (1994) fail to account for the concentration of higher ionization species, a situation that does not improve when similar ICF's available in the literature are considered. A better determination of the abundance of oxygen is probably obtained using the ICF prescribed when most of helium is doubly ionized, a situation that does not occur in this object. It is also possible that collisional effects are not well determined in such extreme density and temperature conditions.

2. Given the observation of so many highly ionized species and the probable existence of many other unobserved ions, the inadequacy of the ICF's, the possible complication introduced by shocks and the fact that corrections for temperature fluctuations were not considered (Peimbert & Costero 1969), most of the reported abundances must be viewed with skepticism. The helium abundance, at 0.19 – 0.20, seems well established. The probable abundance for other elements is 3.2–5.2 $\times 10^{-4}$ (oxygen), 5.6–14 $\times 10^{-4}$ (nitrogen), 7.6 $\times 10^{-5}$ (neon), 1.1 $\times 10^{-5}$ (sulphur), 6.6 $\times 10^{-6}$ (argon), and 1.7 $\times 10^{-7}$ (chlorine), though larger values for some of these would not be unexpected.

3. It is confirmed that the mean temperatures in the eastern and western lobes are different: the latter is $\sim$ 1500 K colder when T[N II] is considered, $\sim$ 800 K colder in the case of T[O III]. This is related to differences in density: the mean density in the western lobe is higher, and cooling is more efficient in it. This proposition is ratified, locally and globally, when the density and nitrogen temperature maps are confronted.

4. The temperature ratio T[O III]/T[N II] increases as T[N II] lessens. This trend is expressed in a surprisingly good correlation between these quantities, and seems to imply that the O^{+2} and N^+ regions become increasingly more segregated with a decreasing degree of excitation. Though the trend may be understood, such a tight correlation cannot be explained.

5. An image of a planetary nebula in the light of [Ne V] 3426 Å is probably presented for the first time. The line ratio image [Ne V] λ3426/Hβ provides a superb view of the distribution of highly excited gas in NGC 6302. The plasma extends along the equatorial plane in a fashion that suggests a jet nozzle. The degree of excitation initially lessens away from the equatorial plane, but the plasma is then "re-excited" in four arches composing a bipolar morphology centered on a lane bisecting the nebula in its eastern and western lobes.

Comments and suggestions by an anonymous referee greatly improved the quality of this paper. G. Tovmassian kindly gave part of his observing time to obtain some spectral data. Thanks are given to A. Decourchelle and J. L. Sauvageot for the loan of the [Ne V] filter. The staff of San Pedro Mártir provided excellent assistance. Partial support from DGAPA-UNAM project IN-104991 is acknowledged.

REFERENCES

Aller, L. H. 1984, Physics of Thermal Gaseous Nebula (Dordrecht: Reidel)
Aller, L. H., & Czysak, S. J. 1978, Publ. Nat. Acad. Sci., 75, 1
Aller, L. H., Ross, J. E., O'Mara, B. J., & Keyes, C. D. 1981, MNRAS, 197, 95 (ARMK)
Ashley, M. C. B., & Hyland, A. R. 1988, ApJ, 331, 532
Bohigas, J. 1994, A&A, 288, 617 (Paper I)
King, D. J., Scarrott, S. M., & Shirt, J. V. 1985, MNRAS, 213, 11
Kingdon, J., & Ferland, G. J. 1995, ApJ, 442, 714
Kingsburgh, R., & Barlow, M. J. 1994, MNRAS, 271, 257
Lame, N. J., & Ferland, G. J. 1991, ApJ, 367, 208
Manchado, A., Stanghellini, L., & Guerrero, M. A. 1996, ApJ, 466, L95
Mathis, J. S., Torres-Peimbert, S., & Peimbert, M. 1998, ApJ, 495, 328
McKenna, F. C., Keenan, F. P., Kaler, J. B., Wickstead, A. W., Bell, K. L., & Aggarwal, K. M. 1996, PASP, 108, 610
Meaburn, J., & Walsh, J. R. 1980a, MNRAS, 191, 5
_____. 1980b, MNRAS, 193, 631
Oliva, E., Pasquali, A., & Reconditi, M. 1996, A&A, 305, L21
Peimbert, M. 1978, in IAU Symp. 76, Planetary Nebula, ed. Y. Terzian (Dordrecht: Reidel), 215
Peimbert, M., & Costero R. 1969, Bol. Obs. Tonantzintla y Tacubaya, 5, No. 31, 3
Peimbert, M., Luridiana, V., & Torres-Peimbert, S. 1995, RevMexAA, 31, 147
Peimbert, M., Sarmiento, A., & Fierro, J. 1991, PASP, 103, 815
Pottasch, S. R., Martínez-Rodríguez, F. J., Schaeidt, S., Valentijn, E., & Vandenbussche, B. 1996, A&A, 315 L261
Pottasch, S. R., Preite-Martínez, A., Olnon, F. M., Jing-Er, M., & Kingma, S. 1986, A&A, 161, 363
Raymond, J. C., Cox, D. P., & Smith, B. W. 1976, ApJ, 204, 290
Reconditi, M., & Oliva, E. 1993, A&A, 274, 662
Rodríguez, L. F., García-Barreto, J. A., Cantó, J., Moreno, M. A., Torres-Peimbert, S., Costero, R., & Serrano, A. 1985, MNRAS, 215, 353
Rowlands, N., Houck, J. R., & Herter, T. 1994, ApJ, 427, 867
Seaton, M. J. 1979, MNRAS, 187, 73
Shaver, P. A., McGee, R. X., Newton, L. M., Danks, A. C., & Pottasch, S. R. 1983, MNRAS, 204, 53
Shaw, R. A., & Dufour, R. 1996, PASP, 107, 896
Stasinska, G. 1980, A&A, 84, 320

Joaquín Bohigas: Instituto de Astronomía, Observatorio Astronómico Nacional, UNAM, Apartado Postal 877, 22830 Ensenada, B. C., México (jbb@bufadora.astrosen.unam.mx).